# Microwave-Free Dynamic Nuclear Polarization via Sudden Thermal Jumps

Carlos A. Meriles[1,2,*] and Pablo R. Zangara[3,4]
[1]Department. of Physics, CUNY-City College of New York, New York, New York 10031, USA
[2]CUNY-Graduate Center, New York, New York 10016, USA
[3]Universidad Nacional de Córdoba, Facultad de Matemática, Astronomía, Física y Computación, X5000HUA Córdoba, Argentina
[4]CONICET, Instituto de Física Enrique Gaviola (IFEG), X5000HUA Córdoba, Argentina

(Received 26 July 2021; accepted 22 December 2021; published 19 January 2022)

Dynamic nuclear polarization (DNP) presently stands as the preferred strategy to enhance the sensitivity of nuclear magnetic resonance measurements, but its application relies on the use of high-frequency microwave to manipulate electron spins, an increasingly demanding task as the applied magnetic field grows. Here we investigate the dynamics of a system hosting a polarizing agent formed by two distinct paramagnetic centers near a level anticrossing. We theoretically show that nuclear spins polarize efficiently under a cyclic protocol that combines alternating thermal jumps and radio-frequency pulses connecting hybrid states with opposite nuclear and electronic spin alignment. Central to this process is the difference between the spin-lattice relaxation times of either electron spin species, transiently driving the electronic spin bath out of equilibrium after each thermal jump. Without the need for microwave excitation, this route to enhanced nuclear polarization may prove convenient, particularly if the polarizing agent is designed to feature electronic level anticrossings at high magnetic fields.

DOI: 10.1103/PhysRevLett.128.037401

The ability to produce order from disorder is perhaps best captured through the notion of a heat engine, extracting mechanical work—a more organized form of energy—from alternately coupling to hot and cold reservoirs. In magnetic systems, Zeeman order is one such form of energy with low entropic content, and so it is natural to wonder whether a thermal cycle can be exploited to induce spin alignment. That this is actually the case is indirectly suggested by recent caloritronics experiments where spin polarization in a ferromagnet emerges from charge flow across a thermal gradient (the so-called spin Seebeck effect [1]). Yet, extending the governing principles to more general systems remains an outstanding problem, particularly if the polarization target is the nuclear spin ensemble of a nonferromagnetic, nonconductive material host.

Admittedly, there is a long-standing, intimate connection between thermal equilibrium and nuclear spin order, already present in Overhauser's famous proposal to dynamic nuclear polarization [2] (DNP). Indeed, the key to this method lies in the ability to steer the electron spin reservoir away from thermal equilibrium through continuous microwave (mw) excitation; equally critical is the built-in asymmetry between the single and double quantum transition rates governing relaxation in the combined electron-nuclear spin system [3]. Although the search for alternative methods to actively polarize nuclear spins has grown to become itself an active field of research [4–8], microwave-based schemes—relying on the Overhauser effect or other mechanisms such as the solid effect, thermal mixing, or the cross effect—are today the most widespread [9]. In all these methods—including those where spin polarization is optically [10–12] or photochemically [13,14] pumped—the sample remains in contact with a thermal bath at a fixed temperature, hence suggesting there is room for other, conceptually different routes to DNP.

Here, we study a system comprising two dipolarly coupled paramagnetic centers featuring different spin-lattice relaxation times near a level anticrossing. By implementing a thermal cycle featuring sudden temperature jumps, we show the spin of hyperfine-coupled nuclei can be dynamically polarized solely with the use of radio-frequency (rf) pulses adjusted to address a pre-selected pair of states with opposite nuclear (and electronic) spin orientations. Under steady state conditions, the limit nuclear polarization that emerges grows with the electron spin population change induced by the thermal jump.

To introduce some of the key ideas, we first consider the schematic in Fig. 1(a) comprising two separate containers $\sigma$, $\sigma'$, each conducting heat from a surrounding thermal bath with characteristic rates $W_\sigma < W_{\sigma'}$. We assume each container encloses two classes of particles, interconverting from one type to the other at a rate $W_\nu \ll W_\sigma, W_{\sigma'}$. Further, we ask that the equilibrium (combined) number of particles in each enclosure be proportional to the outside bath temperature $\mathcal{T}$, and assume we have at our disposal an external means ("gate") to quickly convert one type of particle into the other provided we also switch the containers they are in.

To "polarize" the containers—i.e., to increase the fractional number of one class of particle over the other—we

 

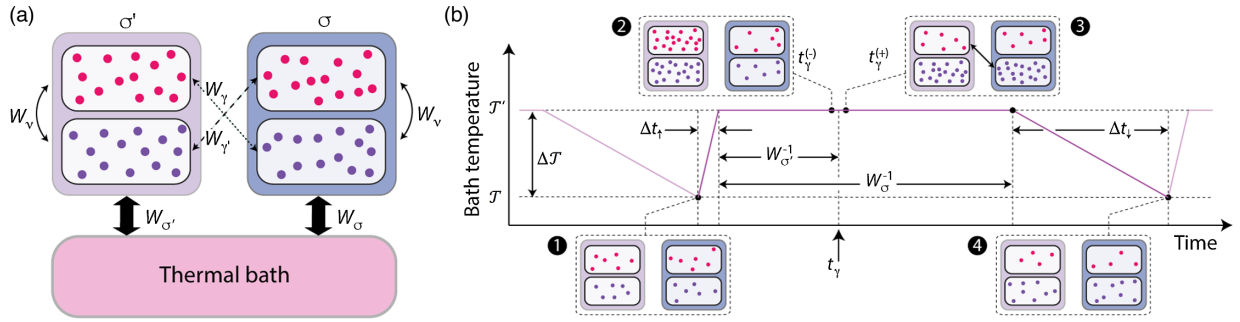


FIG. 1. Dynamic polarization through thermal cycling. (a) We consider two containers exchanging heat with a thermal bath at distinct rates $W_\sigma$, $W_{\sigma'}$. Each container encloses two classes of particles—red and purple—interconverting at a rate $W_\nu \ll W_\sigma$, $W_{\sigma'}$; selective transformation of one class into the other can also be carried out externally at rates $W_\gamma \approx W_{\gamma'} \gg W_\sigma$, $W_{\sigma'}$ provided particles also switch containers (dotted and dashed arrows). In a given container, the total number of particles depends on the container temperature. (b) Starting from a configuration where the number of red and blue particles are the same (stage 1), a sudden thermal jump increases the number of particles in the left container first, thus allowing a gate pulse at $t_\gamma$ to increase the fractional content of blue particles (stages 2 and 3). Since $W_\nu$ is comparatively very slow, the imbalance remains when the bath returns to the original temperature (stage 4).

implement the protocol in Fig. 1(b): Starting from equilibrium at a lower temperature $\mathcal{T}$—where both containers enclose the same (low) number of particles of either type, "stage 1" in the schematic—we quickly heat up the bath to a higher temperature $\mathcal{T}'$. If the timescale of the thermal jump $\Delta t_\uparrow$ is sufficiently short (i.e., when $\Delta t_\uparrow \lesssim W_{\sigma'}^{-1}$), a transient imbalance emerges between the particle populations in each container ["stage 2" in Fig. 1(b)], simply because only one container can thermalize with the bath. At this point, therefore, one can opt to generate polarization of one sign or the other by selectively activating a gate ("stage 3"). Note that the interconversion of particles within each container is slow, implying this polarization is preserved as the system cools back down ["stage 4" in Fig. 1(b)].

Figure 2(a) introduces a physical realization of the above model system in the form of a spin set comprising a hyperfine-coupled nuclear spin $I = 1/2$ and two paramagnetic centers, $S = 1$ and $S' = 1/2$, themselves interacting via a dipolar coupling $\mathcal{J}_d$. We write the system Hamiltonian as

$$H = \Delta S_z^2 - \gamma_e B S_z - \gamma_e B S'_z - \gamma_n B I_z + H_d(S, S') + A_{zz} S_z I_z + A_{zx} S_z I_x, \quad (1)$$

where $\Delta$ is the crystal field acting on spin $S$, and $A_{zz}$ ($A_{zx}$) denotes the secular (pseudosecular) hyperfine coupling constant on the nuclear spin, $\gamma_e$ ($\gamma_n$) is the electronic

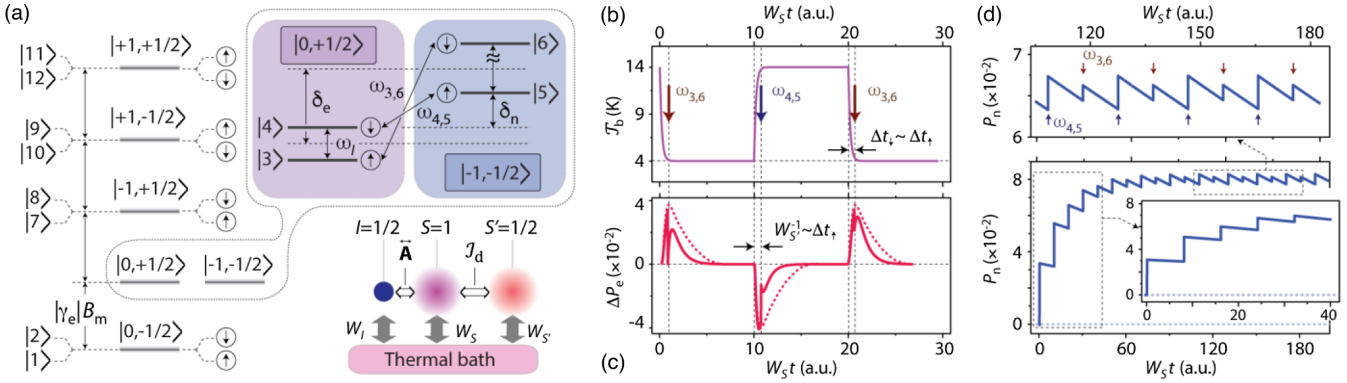


FIG. 2. Thermal cycling near a level anticrossing. (a) Energy level diagram for a spin set formed by two paramagnetic centers with spin numbers $S = 1$, $S' = 1/2$. and a nuclear spin $I = 1/2$ in the vicinity of a level anticrossing. Each spin couples to the thermal bath with characteristic spin-lattice relaxation times $T_{1e}^{(S)} \equiv W_S^{-1}$, $T_{1e}^{(S')} \equiv W_{S'}^{-1}$, and $T_{1n} \equiv W_I^{-1}$, respectively. (b.) Bath temperature $\mathcal{T}_b$ as a function of the normalized time $W_S t$; arrows indicate the application of rf pulses at frequencies $\omega_{45}$ ($\omega_{36}$) during heating (cooling) intervals. (c) Electron spin population difference $\Delta P_e \equiv P_{56} - P_{34}$ as a function of the normalized time; red dotted lines indicate the response in the absence of rf pulses. (d) Nuclear spin polarization as a function of $W_S t$. The upper (lower) insert is a zoomed-out view of the response at late (early) times. Throughout these calculations, we assume $\Delta t_\uparrow = \Delta t_\downarrow = T_{1e}^{(S')} = T_{1e}^{(S)}/5 = T_{1n}/1000 = 10$ ms, $\mathcal{J}_d = 5$ MHz, $A_{zz} = A_{zx} = 10$ MHz, $\delta_e = 30$ MHz, $\delta_n = 10$ MHz, $\Delta = 100$ GHz, and $|\gamma_e|B_m = 50$ GHz; under the above conditions, $\omega_{4,5} = \delta_n = 10$ MHz, $\omega_{3,6} \simeq 58$ MHz.

(nuclear) gyromagnetic ratio, and $H_d(S,S')$ is the dipolar coupling Hamiltonian between spins $S$ and $S'$ [15]. For simplicity, we impose the same (scalar) gyromagnetic ratio $\gamma_e$ to both electron spin species, but assume different spin-lattice relaxation times $W_S^{-1} \equiv T_{1e}^{(S)} > T_{1e}^{(S')} \equiv W_{S'}^{-1}$. The latter is, in general, warranted because the presence of a crystal field in one of the paramagnetic centers creates an asymmetry between the spin-lattice relaxation channels at play for each spin species.

To recreate the polarization protocol in Fig. 1(b), we bring the externally applied magnetic field $B$ to a value near the "matching condition," $|\gamma_e|B_m \equiv \Delta/2$, where the energy splitting between states $|-1\rangle$ and $|0\rangle$ in spin $S$ approximately coincides with the spacing between states $|\pm 1/2\rangle$ in $S'$. While there is some freedom in selecting the exact value of the magnetic field, a practical range emerges from a subtle interplay: On the one hand, we must make the energy detuning $\delta_e = |\gamma_e|(B - B_m)$ greater than a minimum value $\delta_e^{(\min)}$ so that no spontaneous electron-nuclear flip-flops between states $|4\rangle$ and $|5\rangle$ (or $|3\rangle$ and $|6\rangle$) can take place [see Fig. 2(a) for notation]. Conversely, we must make $\delta_e$ smaller than an upper limit $\delta_e^{(\max)}$ so as to ensure reasonably high transition probabilities in the presence of resonant excitation at frequencies $\omega_{4,5}$ or $\omega_{3,6}$. Although nominally forbidden, these transitions—by construction, within the radio-frequency range—activate near the level anticrossing as a result of state hybridization from interspin dipolar and hyperfine couplings, as demonstrated recently [16]. In passing, we caution that the use of exact $\pi$ pulses is not strictly mandatory as the required population exchange could be attained through longer, "saturation" pulses, or via rapid field sweeps that transiently align the energies of the relevant pair of states [17].

Figure 2(b)displays the results from numerical modeling in the case of a spin set featuring hyperfine and dipolar couplings of order 1–10 MHz, typical in organic systems; for presentation purposes, we impose a moderately large crystal field $\Delta = 100$ GHz (corresponding to an approximate matching magnetic field $B_m \approx 1.8$ T), and assume that both the heating and cooling times coincide with the (shorter) spin-lattice relaxation time of spin $S'$, i.e., $\Delta t_\uparrow = \Delta t_\downarrow = T_{1e}^{(S')}$; as discussed later, this condition appears very much compatible with the cryogenic conditions characteristic in current DNP protocols [18].

We readily map the dynamics introduced in Fig. 1 to the spin system at hand when we consider the population difference $\Delta P_e = P_{5,6} - P_{3,4}$ between the integrated electron spin populations $P_{2j-1,2j}$, $j = 2, 3$, as a function of the fractional time $W_S t$ [Fig. 2(c)]. In thermal equilibrium, $\Delta P_e \approx 0$ given the small energy differences (caused by nuclear Zeeman and hyperfine interactions) at the assumed (nearly matching) field. This is no longer the case, however, after a sudden temperature jump because, unlike states $|5\rangle$ and $|6\rangle$, states $|3\rangle$ and $|4\rangle$ can quickly exchange population with ground states $|1\rangle$ and $|2\rangle$ through a flip of spin $S'$, thus inducing a transient population imbalance. For example, during a temperature increase, states $|3\rangle$ and $|4\rangle$ gain population from $|1\rangle$ and $|2\rangle$ whereas the occupancy of states $|5\rangle$ and $|6\rangle$ diminishes from exchange with states $|7\rangle$ and $|8\rangle$, hence leading to $\Delta P_e < 0$. Correspondingly, positive (negative) nuclear polarization follows from the application of an inversion rf pulse at $\omega_{4,5}$ ($\omega_{3,6}$). Further, provided the warm-up and cool-down times $\Delta t_\uparrow$, $\Delta t_\downarrow$ are equally fast—the case in Fig. 2(b)—nuclear polarization of the same sign can be produced following either jump upon switching the rf from one frequency to the other [Fig. 2(d)].

More rigorously, we can derive an approximate expression for the nuclear polarization $P_n = \sum_{j=1}^{6}(P_{2j-1} - P_{2j})$ when we consider the limit case $\Delta t_\uparrow, \Delta t_\downarrow \lesssim T_{1e}^{(S')} \ll T_{1e}^{(S)}$. Assuming the system is initially in equilibrium at temperature $\mathcal{T}$, the transient integrated population $P_{3,4}^{(\mathrm{tr})}$ following a time $t_\gamma^{(-)} \gtrsim T_{1e}^{(S')}$ after a jump to temperature $\mathcal{T}'$ is given by

$$P_{3,4}^{(\mathrm{tr})} \approx (P_{1,2}^{(\mathrm{eq})}|_{\mathcal{T}} + P_{3,4}^{(\mathrm{eq})}|_{\mathcal{T}}) \frac{\exp(-\beta_e')}{[1+\exp(-\beta_e')]}, \tag{2}$$

where $\beta_e' \equiv |\gamma_e|B/k_B\mathcal{T}'$, and $k_B$ denotes Boltzmann's constant. Similarly, the integrated population in states $|5\rangle$ and $|6\rangle$ can be cast as

$$P_{5,6}^{(\mathrm{tr})} \approx (P_{5,6}^{(\mathrm{eq})}|_{\mathcal{T}} + P_{7,8}^{(\mathrm{eq})}|_{\mathcal{T}}) \frac{1}{[1+\exp(-\beta_e')]}. \tag{3}$$

In the above formulas, $P_{2j-1,2j}^{(\mathrm{eq})}|_{\mathcal{T}} = \mathcal{P}\exp[-(E_j/k_B\mathcal{T})]$ denotes the Boltzmann population at temperature $\mathcal{T}$, $E_j$ is the electronic energy in each pair of states $j = 1\ldots6$, and $\mathcal{P}$ is a normalization constant. Equations (2) and (3) express the fact that fractional populations within the $|m_S = 0\rangle$ and $|m_S = -1\rangle$ manifolds reorganize independently after the jump to attain a transient spin temperature, different for each manifold [15]. Therefore, assuming the initial (equilibrium) nuclear polarization is negligible, an rf-induced exchange of the populations in states $|4\rangle$ and $|5\rangle$ yields

$$P_n \approx P_{1,2}^{(\mathrm{eq})}|_{\mathcal{T}} \frac{[1+\exp(-\beta_e)]}{[1+\exp(-\beta_e')]}[\exp(-\beta_e') - \exp(-\beta_e)], \tag{4}$$

where $\beta_e \equiv |\gamma_e|B/k_B\mathcal{T}$. In deriving these expressions, we note that a spin temperature description is warranted at all times during the thermal jump given the comparatively short correlation times of the phonon bath (here serving as the "lattice" [19]).

In the limit where $\exp(-\beta_e)$, $\exp(-\beta_e') \ll 1$, Eq. (4) boils down to $P_n \approx \exp(-\beta_e') - \exp(-\beta_e)$. On the other hand, a thermal jump where $\exp(-\beta_e) \sim 0$ [$\exp(-\beta_e) \sim 1$] and $\exp(-\beta_e') \sim 1$ [$\exp(-\beta_e') \sim 0$] yields the limit warm-up (cool-down) nuclear polarization $|P_{n\uparrow}^{(\max)}| = 1/2$

($|P_{n\downarrow}^{(\max)}| = 1/3$). The asymmetry—still present in intermediate cases, see Fig. 2(d)—stems from the initial population trapped in the $|m_S = +1\rangle$ manifold, nearly null in one case, or approaching $1/3$ of the total in the other. Nuclear polarization of the same magnitude but reversed sign results if the frequencies of the rf pulses in Fig. 2(d) are chosen in the opposite order. Further, while the above discussion assumes $T_{1e}^{(S')} \ll T_{1e}^{(S)}$, identical results follow in the opposite case provided the rf-pulse frequency changes to exchange the populations of states $|3\rangle$ and $|6\rangle$.

Although the above considerations apply exclusively to the hyperfine coupled spin, repeated application of the protocol accompanied by spin diffusion to bulk nuclei—via internuclear couplings or mediated via electron spin interactions [20,21]—will subsequently lead to a net accumulation of nuclear magnetization throughout the sample. The end level of polarization emerges from an interplay between the thermal cycle frequency, the polarization efficiency per cycle, and the spin-lattice relaxation time of bulk nuclei [22]. Note that because Eq. (4) derives exclusively from changes in $\beta_e$, analogous dynamics can be attained if the lattice temperature remains constant and the applied magnetic field cycles between two magnetic fields $B$, $B'$ provided one of the two is proximal to $B_m$. We emphasize that either version of the protocol ultimately relies on the difference between the spin-lattice relaxation times of spins $S$ and $S'$. The implication is that a thermal (or field) jump is fruitless in a system where the polarization source is a single electron spin coupled to a neighboring nucleus, the classical model in DNP.

To better appreciate the practical implications of our approach, it is convenient to draw a comparison with existing nuclear polarization methods. Current DNP technology optimizes polarization gain through a protocol where the sample—prepared to contain a polarizing agent such as TEMPO or related nitroxides [23,24]—is initially frozen to cryogenic temperatures, irradiated with microwave at a moderately strong magnetic field, and then shuttled to a second superconducting magnet for inspection (often after flash thawing). To mitigate the need for sample shuttling, recent efforts have been directed to developing methods adapted to stronger magnetic fields [25]. Work in this front articulates the synthesis of suitable polarizing agents [26,27] and the development of DNP sequences tailored to bring down the required microwave power to a minimum [28].

Without the need for high-power microwave generation—a demanding task at high magnetic fields typically requiring a gyrotron—our approach can nonetheless benefit from the use of cryogenic conditions, because large population changes—and hence high nuclear polarizations—result from even small temperature jumps. This is shown in Figs. 3(a) and 3(b) where we plot the end nuclear polarization in the spin set of Fig. 2 as a function of the thermal jump amplitude $\Delta\mathcal{T} = \mathcal{T}' - \mathcal{T}$ for different base temperatures $\mathcal{T}$. Note that $\Delta\mathcal{T} = \mathcal{T} = 1.5$ K corresponds to conditions entirely within the operating temperature range of the present dissolution DNP experiments [29]. On the other hand, $P_n \approx 10^{-3}$ with a 20 K jump near 80 K, approximately 25 (100) times the $^1$H ($^{13}$C) polarization at 1.8 T at these temperatures.

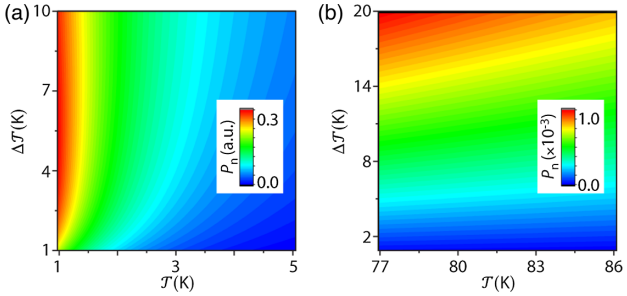


FIG. 3. Thermal dependence. (a) Nuclear spin polarization as a function of the base temperature $\mathcal{T}$ and thermal jump amplitude $\Delta\mathcal{T} = \mathcal{T}' - \mathcal{T}$ for the spin set in Fig. 2. In these calculations, we set $T_{1e}^{(S)} = 5T_{1e}^{(S')} = 50$ ms, $|\gamma_e|B = 50$ GHz. (b) Same as above but near 80 K, corresponding to liquid nitrogen temperatures.

Under the cryogenic conditions assumed above, the spin-lattice relaxation times of typical paramagnetic moieties reach (and often exceed [30,31]) 100 ms, implying that the time interval for a thermal jump can be substantial. For example, bath heating could be quickly enacted by sample illumination with an infrared laser. In particular, we find large end nuclear spin polarization even if $T_{1e}^{(S)}$, $T_{1e}^{(S')}$ differ by as little as a factor 2, and the finite duration of the jump $\Delta t_{\updownarrow}$ is comparable to $T_{1e}^{(S')}$ [15]. As a reference, both heating and cooling jumps with a 50 K amplitude have been recently attained on a 1 $\mu$s time scale in the context of protein folding studies [32]. While this protocol is primarily conceived for nuclear magnetic resonance studies of organic materials, initial demonstrations could benefit from select inorganic platforms. One example is diamond, an excellent thermal conductor where co-existing point defects such as the NV and P1 centers—respectively, featuring spin numbers $S = 1$ and $S' = 1/2$—are known to exhibit different spin-lattice relaxation times [33].

Since the energy level structure near energy matching is largely independent of $B$, we predict only moderate changes in the polarization efficiency at high magnetic fields provided the crystal field also grows proportionally to shift the anticrossing. Further, because the hyperfine couplings of nuclei within the first few atomic shells around a paramagnetic center are large (e.g., 10–150 MHz), practical effective Rabi amplitudes can be attained throughout the range of magnetic fields typical in nuclear magnetic resonance. In particular, it can be shown that, for a fixed thermal jump amplitude, the optimum matching field can be shifted to higher values by raising, not lowering, the base temperature [15].

In summary, we introduced a microwave-free route to dynamic nuclear polarization that builds on the transient imbalance between electron spin populations in nearly degenerate spin levels upon a rapid thermal jump. The end nuclear polarization grows with the difference between the electron spin-lattice relaxation times of the two paramagnetic centers present in the polarizing agent to reach a limit value equal to $1/2$ if the thermal jump amplitude is sufficiently large (though the polarization efficiency drops in the presence of imperfect rf pulses or heterogeneous broadening [15]). Optimal gains can be attained under cryogenic conditions through current DNP instrumentation adapted to produce thermal cycles of small (∼1–10 K) amplitude. Operation at high magnetic fields is possible if one of the paramagnetic centers in the polarizing agent is designed to feature large crystal fields. This could be attained, for example, through the use of molecules pairing a radical and a rare-earth ion, where zero field splittings of up to ∼10 THz are possible [34]. While this work focused on the response under cryogenic temperatures, thermal cycling near ambient conditions may also prove worth exploring. For example, the calculated nuclear polarization after a 50 K jump above room temperature in a 10 T field amounts to $P_n = (|\gamma_e| B/6k_B\mathcal{T})(\Delta\mathcal{T}/\mathcal{T}) \approx 1.5 \times 10^{-3}$, approximately a factor 30 (120) above the equilibrium $^1$H ($^{13}$C) polarization at this field [15].

Work by C. A. M. was supported by the U.S. Department of Energy (DOE), Office of Science, Basic Energy Sciences (BES) under Award No. BES-DE-SC0020638; he also acknowledges access to the facilities and research infrastructure of the NSF CREST IDEALS, Grant No. NSF-HRD-1547830. P. R. Z. acknowledges financial support from SeCyT-UNC (33620180100154CB).

*Corresponding author.
cmeriles@ccny.cuny.edu

[1] K. Uchida, S. Takahashi, K. Harii, J. Ieda, W. Koshibae, K. Ando, S. Maekawa, and E. Saitoh, Observation of the spin Seebeck effect, Nature (London) **455**, 778 (2008).
[2] A. W. Overhauser, Polarization of nuclei in metals, Phys. Rev. **92**, 411 (1953).
[3] C. P. Slichter, *Principles of Magnetic Resonance* (Springer, Berlin 1996).
[4] B. M. Goodson, NMR of laser-polarized noble gases in molecules, materials, and organisms, J. Magn. Reson. **155**, 157 (2002).
[5] J. Natterer and J. Bargon, Parahydrogen induced polarization, Prog. Nucl. Magn. Reson. Spectrosc. **31**, 293 (1997).
[6] T. Theis, P. Ganssle, G. Kervern, S. Knappe, J. Kitching, M. P. Ledbetter, D. Budker, and A. Pines, Parahydrogen-enhanced zero-field nuclear magnetic resonance, Nat. Phys. **7**, 571 (2011).
[7] J. Matysik, A. Diller, E. Roy, and A. Alia, The solid-state photo-CIDNP effect, Photosynth. Res. **102**, 427 (2009).
[8] D. Abrams, M. E. Trusheim, D. Englund, M. D. Shattuck, and C. A. Meriles, Dynamic nuclear spin polarization of liquids and gases in contact with nanostructured diamond, Nano Lett. **14**, 2471 (2014).
[9] B. Corzilius, High-field dynamic nuclear polarization, Annu. Rev. Phys. Chem. **71**, 143 (2020).
[10] V. Jacques, P. Neumann, J. Beck, M. Markham, D. Twitchen, J. Meijer, F. Kaiser, G. Balasubramanian, F. Jelezko, and J. Wrachtrup, Dynamic Polarization of Single Nuclear Spins by Optical Pumping of Nitrogen-Vacancy Color Centers in Diamond at Room Temperature, Phys. Rev. Lett. **102**, 057403 (2009).
[11] K. Ramaswamy, S. Mui, and S. E. Hayes, Light-induced hyperfine $^{69}$Ga shifts in semi-insulating GaAs observed by optically polarized NMR, Phys. Rev. B **74**, 153201 (2006).
[12] J. P. King, Y. Li, C. A. Meriles, and J. A. Reimer, Optically re-writable patterns of nuclear magnetization in gallium arsenide, Nat. Commun. **3**, 918 (2012).
[13] J. H. Lee, A. Sekhar, and S. Cavagnero, 1H-Detected $^{13}$C photo-CIDNP as a sensitivity enhancement tool in solution NMR, J. Am. Chem. Soc. **133**, 8062 (2011).
[14] B. Shapira, E. Morris, K. A. Muszkat, and L. Frydman, Sub-second 2D NMR spectroscopy at sub-millimolar concentrations, J. Am. Chem. Soc. **126**, 11756 (2004).
[15] See Supplemental Material at http://link.aps.org/supplemental/10.1103/PhysRevLett.128.037401 for details on the system Hamiltonian, the spin dynamics during a thermal jump, the polarization efficiency, and the response at high temperatures.
[16] P. R. Zangara, D. Pagliero, A. Ajoy, R. H. Acosta, J. A. Reimer, and C. A. Meriles, Nuclear spin temperature reversal via continuous radio-frequency driving, Phys. Rev. B **103**, 085205 (2021).
[17] J. Henshaw, D. Pagliero, P. R. Zangara, B. Franzoni, A. Ajoy, R. Acosta, J. A. Reimer, A. Pines, and C. A. Meriles, $^{13}$C dynamic nuclear polarization in diamond via a microwave-free 'integrated' cross effect, Proc. Natl. Acad. Sci. U.S.A. **116**, 18334 (2019).
[18] *Handbook of High Field Dynamic Nuclear Polarization*, edited by V. K. Michaelis, R. G. Griffin, B. Corzilius, and S. Vega (John Wiley, and Sons, New York, 2020).
[19] M. Goldman, Formal theory of spin–lattice relaxation, J. Magn. Reson. **149**, 160 (2001).
[20] D. Pagliero, P. R. Zangara, J. Henshaw, A. Ajoy, R. H. Acosta, N. Manson, J. A. Reimer, A. Pines, and C. A. Meriles, Magnetic-field-induced delocalization in hybrid electron-nuclear spin ensembles, Phys. Rev. B **103**, 064310 (2021).
[21] D. Pagliero, P. Zangara, J. Henshaw, A. Ajoy, R. H. Acosta, J. A. Reimer, A. Pines, and C. A. Meriles, Optically pumped spin polarization as a probe of many-body thermalization, Sci. Adv. **6**, eaaz6986 (2020).
[22] P. R. Zangara, J. Henshaw, D. Pagliero, A. Ajoy, J. A. Reimer, A. Pines, and C. A. Meriles, Two-electron-spin ratchets as a platform for microwave-free dynamic nuclear polarization of arbitrary material targets, Nano Lett. **19**, 2389 (2019).
[23] D. A. Hall, D. Maus, G. J. Gerfen, and R. G. Griffin, Polarization-enhanced NMR spectroscopy of biomolecules in frozen solution, Science **276**, 930 (1997).

[24] J. H. Ardenkjaer-Larsen, B. Fridlund, A. Gram, G. Hansson, L. Hansson, M. H. Lerche, R. Servin, M. Thaning, and K. Golman, Increase in signal-to-noise ratio of >10, 000 times in liquid-state NMR, Proc. Natl. Acad. Sci. U.S.A. **100**, 10158 (2003).

[25] T. Maly, G. T. Debelouchina, V. S. Bajaj, K.-N. Hu, C.-G. Joo, M. L. Mak–Jurkauskas, J. R. Sirigiri, P. C. A. van der Wel, J. Herzfeld, R. J. Temkin, and R. G. Griffin, Dynamic nuclear polarization at high magnetic fields, J. Chem. Phys. **128**, 052211 (2008).

[26] A. Equbal, K. Tagami, and S. Han, Balancing dipolar and exchange coupling in biradicals to maximize cross effect dynamic nuclear polarization, Phys. Chem. Chem. Phys. **22**, 13569 (2020).

[27] F. Mentink-Vigier, Optimizing nitroxide biradicals for cross-effect MAS-DNP: The role of $g$-tensors' distance, Phys. Chem. Chem. Phys. **22**, 3643 (2020).

[28] K. O. Tan, C. Yang, R. T. Weber, G. Mathies, and R. G. Griffin, Time-optimized pulsed dynamic nuclear polarization, Sci. Adv. **5**, eaav6909 (2019).

[29] D. Gajan, A. Bornet, B. Vuichoud, J. Milani, R. Melzi, H. A. van Kalkeren, L. Veyre, C. Thieuleux, M. P. Conley, W. R. Grüning, M. Schwarzwälder, A. Lesage, C. Copéret, G. Bodenhausen, L. Emsley, and S. Jannin, Hybrid polarizing solids for pure hyperpolarized liquids through dissolution dynamic nuclear polarization, Proc. Natl. Acad. Sci. U.S.A. **111**, 14693 (2014).

[30] M. Kveder, D. Merunka, M. Jokić, J. Makarević, and B. Rakvin, Electron spin-lattice relaxation in solid ethanol: Effect of nitroxyl radical hydrogen bonding and matrix disorder, Phys. Rev. B **80**, 052201 (2009).

[31] C. Hess, J. Herick, A. Berlin, W. Meyer, and G. Reicherz, Measurement of electron spin-lattice relaxation times in radical doped butanol samples at 1 K using the NEDOR method, Nucl. Instrum. Methods Phys. Res., Sect. A **694**, 69 (2012).

[32] M. E. Polinkovsky, Y. Gambin, P. R. Banerjee, M. J. Erickstad, A. Groisman, and A. A. Deniz, Ultrafast cooling reveals microsecond-scale biomolecular dynamics, Nat. Commun. **5**, 5737 (2014).

[33] S. Takahashi, R. Hanson, J. van Tol, M. S. Sherwin, and D. D. Awschalom, Quenching Spin Decoherence in Diamond through Spin Bath Polarization, Phys. Rev. Lett. **101**, 047601 (2008).

[34] K. Binnemans, Interpretation of Europium(III) spectra, Coord. Chem. Rev. **295**, 1 (2015).